



CrossMark
click for updates

Cite this: DOI: 10.1039/c6tc05122g

Impact of ultrathin dielectric spacers on SERS: energy transfer between polarized charges and plasmons†

D. R. Nayak,^a N. Bhat,^{ab} M. Venkatapathi^c and S. Umamathy^{*de}

The optical properties of plasmonic nanoparticles and substrates have been exploited to produce vapour deposited substrates that are as effective as SERS substrates produced using sophisticated nanolithography. In this work, we show that introducing ultrathin dielectric spacers of ~ 5 nm between the silicon substrate and the silver nanoparticles provides adequate screening and allows for energy transfer between the plasmons and polarization charges of the high-permittivity silicon, a desirable feature for SERS enhancement. We show this effect using different dielectric spacers of silicon dioxide, silicon nitride and others. Note that the energy transfer process is active for distances < 10 nm and falls as $1/d^6$ (where d is the thickness of the spacer), and larger spacers asymptotically approach the radiative regime of thin-film interference with an intermediate non-radiative regime ($d \sim 10$ – 40 nm). Enhancement of Raman scattering signals by factors close to 10^5 has been observed from these substrates that can be easily produced on large areas. The experimental studies were complemented by COMSOL numerical results showing the shifting and enhancement of plasmon resonances of the silver particles due to the spacers predicting similar enhancements. We also present a radiation model of the silicon substrate and silver particles with an interleaving boundary-layer of such induced permittivity that predicts these experimental observations equally well.

Received 25th November 2016,
Accepted 2nd February 2017

DOI: 10.1039/c6tc05122g

rsc.li/materials-c

Introduction

Optical confinement in sub-100 nm metal structures has been a field of extensive research in the past decade. The tunable optical properties of these nanostructures cover a wide range of applications.¹ Metallic nanoparticles and nanostructures give rise to a collective surface electron resonance (plasmon resonance) due to the oscillating electric field of the incident electromagnetic wave. The resonance condition of the free electron oscillation depends on the wavelength of the incident

electromagnetic wave, the optical properties of the metal and the properties of the proximal environment.^{2–4} The shape of the metal structure defines the surface plasmon resonance to be propagating or confined. Nanoparticles result in localised surface plasmon resonance (LSPR) which in turn couples to the incident wave to give rise to an intense electric field in the vicinity of its surface. Performing Raman spectroscopy while the analyte molecules experience this intense electric field enhances the weak Raman signal by many orders of magnitude.^{5–7} This forms the basis of surface enhanced Raman spectroscopy (SERS) using substrates deposited with metal nanoparticles.

To perform SERS, it is vital to have the LSPR of the nanostructure coincide with the probed wavelength. The plasmonic property is vastly influenced by the local environment which results in shifting of the LSPR peak. The plasmonic particle on a conducting or insulating substrate couples to the propagating SPR or to the image of itself respectively.^{8–11} In the case of an insulating substrate, the strength of the image of the plasmonic nanoparticle formed on the substrate depends on its permittivity. A stronger image screened by the substrate, due to higher permittivity, results in larger enhancement as well as a shift in the LSPR peak.^{10,12–16} Some of the earlier reports have attempted to quantify the image effect by inserting a spacer layer between the nanoparticle and the bulk substrate.^{8,10} However, these

^a Centre for Nanoscience and Engineering, Indian Institute of Science, Bangalore, 560012, India

^b Department of Electrical and Communication Engineering, Indian Institute of Science, Bangalore, 560012, India

^c Computational & Statistical Physics Laboratory, Department of Computational & Data Sciences, Indian Institute of Science, Bangalore, 560012, India

^d Department of Inorganic and Physical Chemistry, Indian Institute of Science, Bangalore, 560012, India

^e Department of Instrumentation and Applied Physics, Indian Institute of Science, Bangalore, 560012, India. E-mail: siva.umamathy@gmail.com

† Electronic supplementary information (ESI) available: Computational methods and results; inter-particle coupling; the extinction cross-section of AgNPs on different substrates; particle volume density; optimization of the Wind model; ellipsometry results; normal Raman spectra and peak assignment; and comments on the accuracy of the enhancement mechanism. See DOI: 10.1039/c6tc05122g

effects have been studied with respect to the bulk substrate permittivity, mostly ignoring the spacer layer or its thickness.

This paper presents a combined experimental and theoretical study of very thin dielectric spacers that may provide the induced polarization/permittivity required to allow effective energy transfer between plasmons of nanoparticles and the bulk substrate. The energy screened by the bulk substrate would be a function of the thin film permittivity. The results include the effect of both the spacer and the base substrate which is distinct from the earlier works on such models.^{10–12,17–19} Our experimental and numerical results on spacers comparable to the wavelength in dimensions are discussed elsewhere. Different thin films (SiO_2 , HfO_2 , Si_3N_4 , and SiC) were deposited on the $\text{Si}(100)$ substrate and subsequently silver nanoparticles were created on top of these substrates by means of sputtering. SERS was performed on these substrates with pyridine to identify the enhancement variation. The cross-sections of nanoparticles on the substrate for each case have been simulated using COMSOL Multiphysics 4.3b. An analytical model has been formulated to take the substrate-spacer effect into account. This model's prediction of the low energy mode LSPR peak and that obtained from computation have been compared for robustness. The model includes the nanoparticle size dependent shift and predicts relatively accurate dipolar mode positions for gold nanoparticles as well.²⁰ The results show significant changes in the SERS intensity with respect to the spacer layer permittivity with silicon. This presents a simple scalable process technique to enhance the SERS signal by inserting an appropriate thin spacer layer on standard substrates such as Si wafer.

Results and discussion

Experiments were carried out to understand the influence of the permittivity of the spacer layer on the nanoparticles. Films of SiO_2 , Si_3N_4 , HfO_2 and SiC with a thickness of 5 nm were deposited on a pristine $\text{Si}(100)$ substrate. The thicknesses and the refractive index values were obtained by spectroscopic ellipsometry. The model used for the analysis of the refractive index and thickness is discussed in the ESI.† The refractive indices of different materials are listed in Table S3 of the ESI.† On all the substrates, about 6 nm of Ag was sputtered followed by thermal annealing to create nanoparticles. The deposition time and annealing parameters were optimized to obtain similar distribution of nanoparticles on all the substrates. Fig. 1 shows nanoparticles on different substrates and their size distribution. The average size of the nanoparticles on all substrates was about 10 nm to 14 nm with a range from 4 nm to 24 nm. It is evident from the SEM images that the nanoparticle density is approximately the same for the substrates with Si_3N_4 , SiO_2 , and HfO_2 spacers with the exception of the SiC spacer substrate. Given the quasi-static limit of the nanoparticle size, the resonance efficiency is mainly dependent on the absorption of the nanoparticles and scales with the volume (eqn (6)). Hence, the metal volume density represents the SERS intensity accurately rather than the particle density (for details, refer the ESI.†).

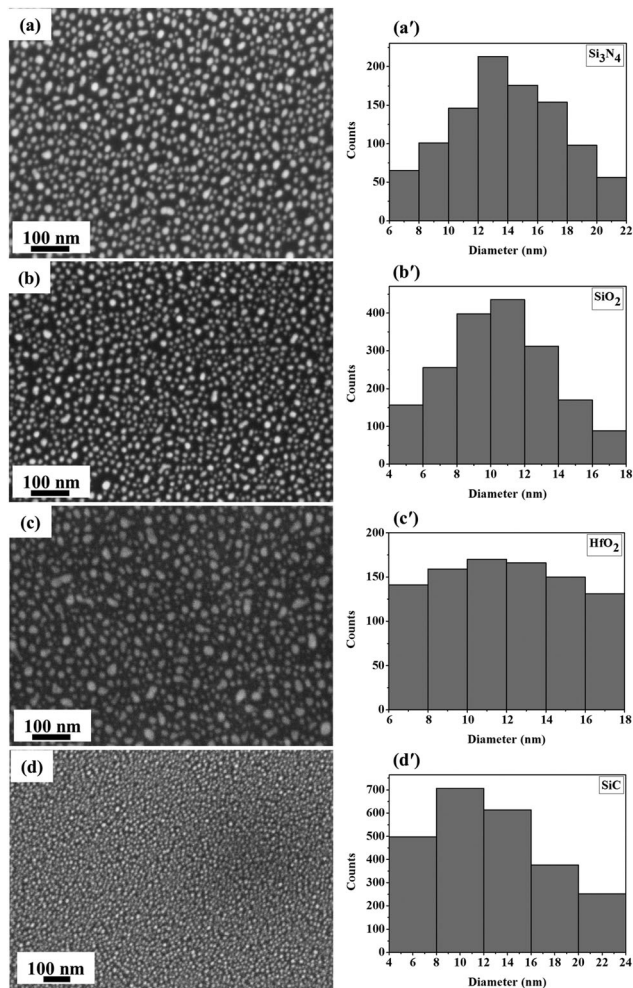


Fig. 1 Nanoparticles of Ag on substrates with 5 nm films of (a) Si_3N_4 , (b) SiO_2 , (c) HfO_2 and (d) SiC with the corresponding size distribution from a'–d' respectively.

This assumption is also reflected in the experimental data presented in Fig. 6a, which show that the SERS intensity is comparatively less in the SiC spacer substrate despite the higher particle density. The volume densities of the substrates are provided in the ESI.† for comparison. The fabrication and experimental parameters are discussed in the Experimental section.

The SERS signal of pyridine solution was obtained on the fabricated substrates at 532 nm and 633 nm laser excitation. Multiple SERS spectra were obtained from different spots on the substrate. All spectra were averaged and the standard errors for the peaks were calculated. One such representation is shown in Fig. 2a which is an average spectrum with standard error plotted for 1007 cm^{-1} and 1036 cm^{-1} Raman peaks. Pyridine has characteristic Raman peaks at 1007 cm^{-1} and 1036 cm^{-1} corresponding to ring breathing and symmetric ring deformation modes respectively.²¹ The intensity of the 1036 cm^{-1} peak was compared for different substrates for a particular excitation wavelength. The average of the 1036 cm^{-1} peak in Fig. 2a corresponds to the datapoint plotted against the Si_3N_4 substrate in Fig. 2b. As shown in Fig. 2b, the substrate with a Si_3N_4

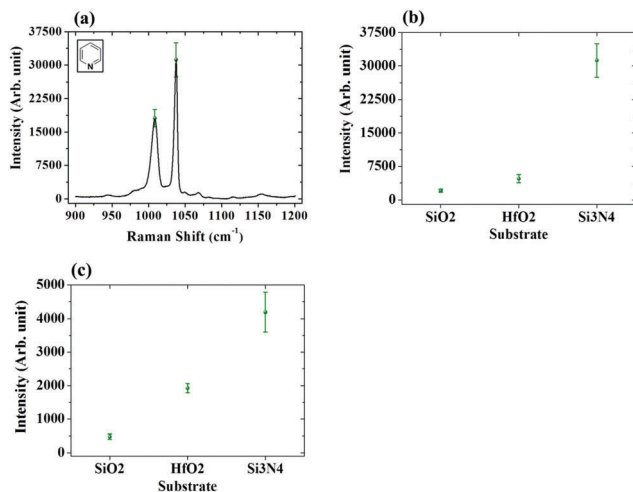


Fig. 2 (a) Average SERS spectra obtained from the substrate with 5 nm Si_3N_4 films probed with a 532 nm laser. The inset shows the pyridine molecule. SERS intensity comparison of the 1036 cm^{-1} band on different substrates probed with (b) 532 nm and (c) 633 nm wavelength lasers.

spacer gives the highest SERS intensity. The trend observed for increasing SERS intensity with the increase in the spacer permittivity was also confirmed at 633 nm laser excitation (Fig. 2c).

The SERS intensity depends on the absorption cross-section of the nanoparticles which is different for different substrates. Experimentally observing the LSPR modes is challenging which is discussed in detail in the ESI† Hence, computation was carried out using COMSOL using the electromagnetic waves (frequency domain) module to determine the LSPR peak of a silver hemisphere on a substrate and the change in its position and amplitude with respect to change in the spacer layer permittivity. One of the simulations with an Ag hemisphere on 5 nm SiO_2 on Si is shown in Fig. 3. The simulation domain consists of one nanoparticle on a substrate instead of multiple particles in order to decrease the computation cost. This takes into account the well-known attribute that the distance between the surfaces of two particles for inter-particle plasmon coupling is $\ll a$, the dimension of the particle. The coupling distance reduces drastically as the nanoparticle size decreases. Simulation results of a 14 nm nanoparticle on a Si_3N_4 spacer substrate showed considerable coupling below 3 nm (Fig. S5, ESI†). It is valid to assume

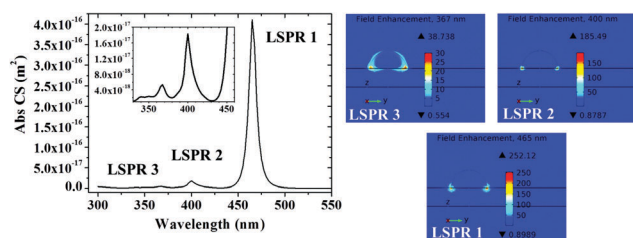


Fig. 3 Absorption cross-section and LSPR modes of a 10 nm Ag hemisphere on a 5 nm SiO_2 spacer on a Si substrate. The inset shows the scaled region of the plot for visualization of LSPRs 2 and 3. The field enhancement in the individual resonance condition is depicted in the color plots.

that the nanoparticles smaller than 14 nm will have coupling only below 3 nm inter-particle distance. Computed cross-sections show a red-shift of the LSPR modes for Ag nanoparticles on a substrate with higher permittivity compared to the substrate with a 5 nm SiO_2 film (Fig. S6, ESI†). The probed wavelength of 532 nm is favourable towards the substrates with Si_3N_4 and HfO_2 films which is observed from the experimental data in Fig. 2b. Although the calculated LSPR peaks do not coincide with the excitation at 633 nm for all the substrates, the intensity profile with respect to the permittivity of the dielectric layer remains the same (Fig. 2b). An analytical model has been formulated in order to compute the exact effect of the coupling of LSPR of the nanoparticle and the image charge formed on the substrate.

Out of the three modes of the hemisphere, the intense lower order or the first mode has higher substrate dependence than other modes. The analytical model has been formulated using earlier calculations^{22,23} to account for the substrate effect on the LSPR amplitude and peak position in the first mode. The model explicitly takes the image charge effect into account. The strength of the image charge is proportional to the permittivity of the spacer. The coupling of surface plasmons with its image charge, termed the Coulomb effect, causes the resonance mode to red-shift with an increase in permittivity. The Coulomb effect also results in an increase in the near field enhancement resulting in high SERS intensity. However, a radiative effect can be expected from thicker films which will result in a change in the resonance intensity rather than the peak shift.^{17,24} This effect arises due to the coupling of a fraction of the electromagnetic wave to the substrate and becomes prominent as the spacer thickness increases.^{17,18} In the present discussion, the electrostatic or Coulomb effect prevails as the film thickness is only 5 nm. Apart from the direct effect of the film permittivity, a fraction of the base substrate permittivity is observed to play a significant role in the LSPR modulation. The contribution arises due to non-radiative energy transfer from the nanoparticle to the silicon base substrate screened by the spacer film. This causes a dipole-dipole interaction between the nanoparticle and silicon. The dipole-dipole interaction is modeled in eqn (2). The nanoparticle lies closer to the Si base substrate for ultra-thin (< 10 nm) spacer layers. As the spacer thickness increases, the coupling to the base substrate decreases as $1/d^6$, and the effect is purely due to the Coulomb interaction between the nanoparticle and the film. This is evident from Fig. 4a where the LSPR does not shift for a higher thickness of the film. The simulation was carried out at a constant film permittivity, irrespective of the thickness, to decouple any screening effect from the film. The plasmon resonance in the nanoparticle polarizes the semi-conducting substrate partially for a spacer with thickness < 10 nm which is termed as the energy transfer (Fig. 4b). The analytical model captures the effect by formulating an effective substrate with permittivity of the film and the $1/d^6$ factor (filling factor in eqn (2)) of the Si permittivity. The values of the filling factor can be varied from 0 to 1 resulting in pure silicon permittivity and pure film permittivity, respectively, through eqn (1). The methods are explained in detail in the Analytical modelling section. The higher thickness regime ($> \sim 10$ nm)

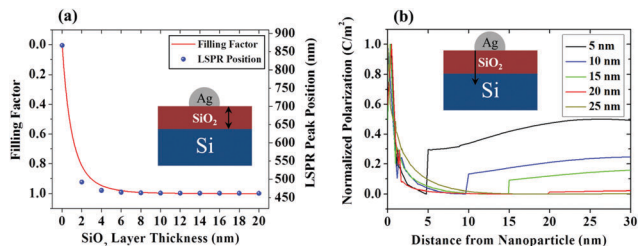


Fig. 4 (a) Comparison of the filling factor (eqn (2)) and the LSPR shift as the spacer thickness increases. Schematic of the simulation domain is shown in the inset. (b) Normalized magnitudes of polarization of the spacer and the substrate for different spacer thicknesses. Inset shows the direction of the COMSOL line plot *i.e.*, the arrow length corresponds to the x -axis of the plot.

has been experimentally explored in our other work which suggested an intermediate non-radiative regime (~ 10 – 40 nm) which depends only on the film permittivity. As the thickness increases, a radiative regime of thin-film interference is observed to be dominant and can be modelled well with standard equations.²⁵

The absorption cross-sections obtained from both the computation and the analytical model were compared with the experimental results by reducing the actual data to a relative gain factor. The experimental gain was obtained by dividing the SERS intensity of a substrate by that of the substrate with a SiO₂ film in Fig. 2b and c for different wavelengths. The calculated gains were the ratios of absorption cross-sections of a substrate and a substrate with a SiO₂ film. The ratio reduces all the quantities to a dimensionless number which predicts the efficiency of a substrate with respect to the substrate with the SiO₂ film. The prediction of gains calculated from the cross-section values were in close agreement with the experimentally obtained gain (Fig. 5). The modelling revealed that the enhancement at 532 nm may be due to the LSPR peak positions but at 633 nm the enhancement corresponds to the Coulomb effect. The intensity in the off-resonance regime will be a strong function of substrate permittivity.

An experiment was carried out to confirm the permittivity effect in the case of a SiC spacer at 514 nm (Fig. 6a). The permittivity of the SiC film at 514 nm is 6.07 which is about three times that of the Si₃N₄ film. Theoretically, the LSPR mode in SiC substrates will be highly red-shifted compared to the Si₃N₄ substrate (Fig. S6, ESI[†]). Hence, 514 nm falls in the off-

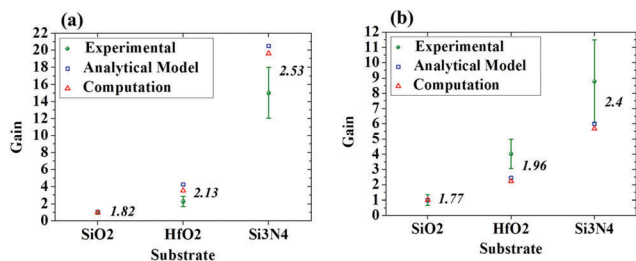


Fig. 5 Comparison of gain in SERS intensity predicted by the proposed analytical model, COMSOL and the experimental gain with respect to the SiO₂ substrate at (a) 532 nm and (b) 633 nm wavelength laser. (Permittivities of the films are italicized.)

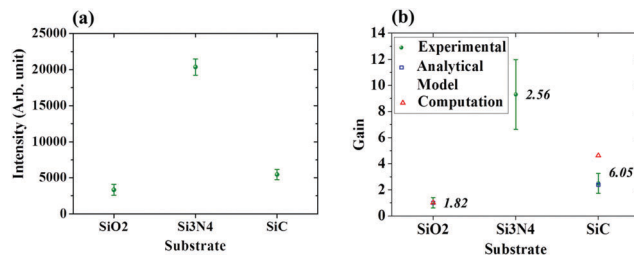


Fig. 6 Comparison of (a) SERS intensity of different substrates and (b) gains probed with a 514 nm laser. (Permittivities of the films are italicized.)

resonance regime for the SiC substrate but coincides with the resonance of the Si₃N₄ substrate. The experimental results confirm that the enhancement is proportional to the substrate permittivity only in the off-resonance region, as predicted before, when SiO₂ and SiC substrates are compared (Fig. 6b). If resonance conditions are met for a particular substrate, the enhancement will not follow the permittivity trend. The gain calculated by computation and using the analytical model failed to predict the experimental observation at 514 nm which is discussed in the ESI[†] (Fig. S6). This contradiction may be due to calculation near to the resonance region which resulted in significant gain for the Si₃N₄ substrate, but the experimental observations remain close to the predicted trend obtained from the calculation. Semiconducting films *e.g.*, SiC may show non-optical quenching, which has been attributed to the possibility of electron exchange between a metal nanoparticle and a semiconducting substrate.¹⁹

Experimental SERS gains from the substrates are expected to follow the prediction for various analytes, but may differ by a few factors as SERS enhancements of all Raman bands are not identical. The adsorption mechanism,^{26,27} electric field variation^{28,29} and surface selection rules^{30,31} are a few of the aspects which contribute to dissimilar enhancement among bands of an analyte. The calculated prediction proposes an average relative gain of a substrate for a general case.

The substrate with 5 nm of a Si₃N₄ film showed better performance than other substrates. Hence the substrate was used for further characterization with *p*-nitrophenol (PNP) and Rhodamine 6G (R6G) to obtain the enhancement factor (Fig. 7a and c). The Raman peak of PNP at 1116 cm⁻¹ corresponding to C–H in-plane bending motion^{32–34} and the peak of R6G at 1181 cm⁻¹ corresponding to in-plane xanthene ring deformation^{35,36} were taken into account for the calculation of an analytical enhancement factor⁷ which was found to be in the range of 10⁴ to 10⁵ (Tables S4 and S5 in the ESI[†] provide details on mode assignment for various peaks). The results were comparable to SERS substrates with various nanostructures fabricated by e-beam lithography.^{37,38} SERS results with PNP showed better performance on substrates with Si₃N₄ as compared to SiO₂. In order to check the reproducibility, SERS spectra were acquired from several spots across the substrates. The averaged spectrum is plotted in Fig. 7c with standard error (red), which suggests that the intensity variations are within 7%. The obtained individual spectra are provided in Fig. 7d as an intensity contour map.

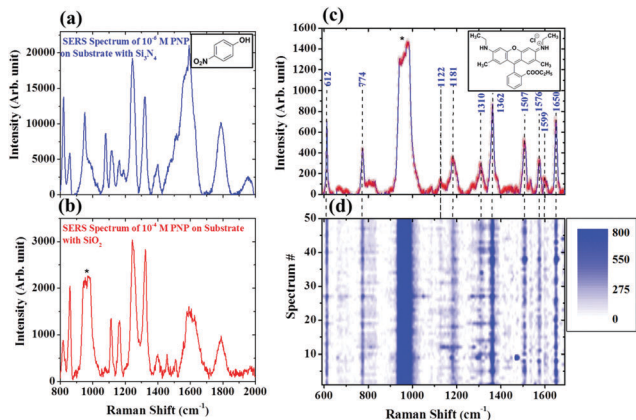


Fig. 7 SERS spectrum of (a) 10^{-6} M PNP on a substrate with Si_3N_4 (inset: PNP) and (b) 10^{-4} M PNP on a substrate with SiO_2 . (c) Averaged SERS spectrum with standard error from 10^{-7} M R6G (inset: R6G) and (d) SERS intensity contour of all individual spectra obtained from the substrate with Si_3N_4 . Asterisks correspond to the second-order peak from the Si substrate.³⁹

Experimental

Materials and methods

Si_3N_4 , HfO_2 and SiC films of 5 nm thickness were deposited on pristine $\text{Si}\langle 100 \rangle$ by low pressure chemical vapour deposition (ET-6000, First Nano), RF magnetron sputtering (Tecport) and plasma enhanced chemical vapour deposition (Plasma Labsystem 100, Oxford Instruments) respectively. SiO_2 of 5 nm thickness was thermally grown on Si (ET-6000, First Nano). Spectroscopic ellipsometry (M200U, J.A. Woollam Co.) was performed to measure the thickness and refractive index of the films. On all the substrates, about 6 nm of Ag was sputtered using DC magnetron sputtering (Tecport) followed by thermal annealing (ET-6000, First Nano) in a nitrogen atmosphere for 10 minutes at 300 °C. Pyridine solution was dispersed on the substrates with a micropipette and the SERS spectra were recorded with a 50 \times LWD objective. Spectra in Fig. 2a and b were recorded for 0.1 M pyridine with acquisition for 1 s using a LabRAM HR800 equipped with a 1800 grooves per mm grating and a 532 nm laser. Spectra in Fig. 2c were recorded for 0.01 M pyridine with an acquisition time of 1 s using a Renishaw in-Via series equipped with a 1200 grooves per mm grating and a 633 nm laser. Spectra in Fig. 6a were recorded for 0.1 M pyridine with acquisition for 1 s using a LabRAM HR800 equipped with a 1800 grooves per mm grating and a 514 nm laser. Spectra in Fig. 7a and b were recorded with an acquisition time of 10 s using a Renishaw inVia series equipped with a 2400 grooves per mm grating and a 514 nm laser. Spectra in Fig. 7c were obtained with an acquisition time of 5 s.

COMSOL simulation

The cross-section calculation of the nanoparticle was carried out by defining the background electromagnetic wave. The background wave was first calculated by sweeping wave from port without the presence of the nanoparticle with Floquet periodic boundary condition. The resultant field was used to calculate the cross-sections in a second domain of simulation

with the nanoparticle on the substrate. The details of the simulation domain schematics and the equations used for the calculation of cross-sections are discussed in the ESI.[†] The simulation result gave a reasonable estimation of the peak positions (Table S1, ESI[†]).

The charge distribution on the nanoparticle defines the mode of resonance. The hemisphere in homogeneous media exhibits three modes of LSPR when excited with polarization parallel to the cutting plane (Fig. S3, ESI[†]). The peaks are numbered in ascending order from a low energy peak to a high energy peak. Keeping the hemisphere on a substrate does not break the symmetry as reported elsewhere.⁴² This report is in contrast to the case of a sphere on a substrate where additional peaks are observed due to symmetry breaking and surface modes.^{43–46} The substrate interaction causes the three peaks to shift from the LSPRs observed in the case of the hemisphere in a homogenous medium. The substrate has a minute effect on the high energy LSPR or the third peak. This can be intuitively explained as the plasmons accumulating on the top spherical surface in this mode and experiencing a comparatively lower effect from the substrate. The second and the first LSPR modes show considerable charge accumulation on the flat side of the hemisphere. This is affected by the substrate as the image charge formed in the bulk substrate couples to the plasmons.^{12,47} LSPRs of the Ag hemisphere on different bulk substrates (without films) show varying degrees of red-shift which is proportional to the permittivity of the underlying substrate (Fig. S7, ESI[†]). SiO_2 shows the least amount of shift whereas Si shows the highest. Due to the presence of near field enhancement factors, the first LSPR peak is considered for subsequent analytical modelling. The equations in analytical modelling are derived using image charge theory which can predict the actual contribution for the same reason.

Analytical modelling

The substrate under study consists of bulk Si on which 5 nm of the film is deposited. It is difficult to account for the image charge formed on both bulk (Si) and the film (spacer). Hence, an effective model is necessary to convert the bulk Si with a 5 nm film to a single substrate with an effective permittivity. Maxwell Garnett formulated effective medium approximation for inclusions in a homogenous medium⁴⁸ which was later reformulated for inclusions which are finite in two dimensions.⁴⁹ The equation is approximated for inclusion of the film which is finite in one dimension (eqn (1)). The filling factor (f) corresponds to the volume fraction of the film. The extent of the film in two dimensions is optically infinite, so it is reasonable to take only the thickness ratio into account for calculation of the volume fraction. The total thickness taken into account should correspond to the radiation extent of a specific resonance mode of the nanoparticle in the substrate.

The radiating field is purely electric in nature near the dipole.⁵⁰ The radiation extent denotes the extent of this electrostatic field from the nanoparticle surface. The radiation decay from the nanoparticle is assumed to be a^6 , where a is the radius of the nanoparticle. This assumption is based on the

energy transfer model and correlates well with the results of computation (Fig. 4a).

A continuous formula is proposed in eqn (2) for calculation of the filling factor. To avoid singularity, the calculation is done by representing the dipole at an $\frac{a}{2}$ distance above the substrate. The results match the effects observed in the computation.

$$\frac{\epsilon_{\text{effs}}(\lambda) - \epsilon_{\text{Si}}(\lambda)}{\epsilon_{\text{effs}}(\lambda)} = f \left(\frac{\epsilon_{\text{f}}(\lambda) - \epsilon_{\text{Si}}(\lambda)}{\epsilon_{\text{f}}(\lambda)} \right) \quad (1)$$

$$f = \frac{\int_{\frac{a}{2}}^{d+\frac{a}{2}} \frac{1}{l^6} dl}{\int_{\frac{a}{2}}^{\infty} \frac{1}{l^6} dl} \quad (2)$$

The terms ϵ_{effs} , ϵ_{Si} , and ϵ_{f} are the permittivities of the effective substrate, Si and film respectively.

The polarizability of the silver hemisphere on the calculated effective substrate was obtained using the analytical solution formulated by Wind *et al.*²² The analytical solution incorporates the image charge formation on the substrate. The solution to polarizability of a hemisphere on a substrate contains the B_{11} term which is calculated using eqn (3).

$$B_{11} = \frac{(\epsilon_{\text{m}} + \epsilon_{\text{effs}})(\epsilon_{\text{m}} - \epsilon_{\text{Ag}})}{2\epsilon_{\text{m}}(2\epsilon_{\text{m}} + 3\epsilon_{\text{effs}} + \epsilon_{\text{Ag}})} \quad (3)$$

where ϵ_{m} , ϵ_{effs} and ϵ_{Ag} are the permittivities of the medium, substrate and silver respectively.

The above analytical formula has been modified by the inclusion of a size factor (sf). The size factor incorporates resonance shift due to the size of the nanoparticle. The size factor, which is a function of the propagation constant (k) and the diameter of the nanoparticle, for the Fröhlich frequency has been modified to match substrate conditions.⁵¹

$$B_{11} = \frac{(\epsilon_{\text{m}} + \epsilon_{\text{effs}})(\epsilon_{\text{m}} - \epsilon_{\text{Ag}})}{2\epsilon_{\text{m}}(\text{sf} \times 2\epsilon_{\text{m}} + \text{sf} \times 3\epsilon_{\text{effs}} + \epsilon_{\text{Ag}})} \quad (4)$$

$$\text{sf} = 0.83 + \frac{12}{5}x^2; \quad x = k \times \text{dia} \quad (5)$$

Eqn (4) predicts only the lowest energy LSPR mode or the first mode of the hemisphere on the substrate. The volume polarizability of a hemisphere on a substrate for perpendicular incidence²² and the absorption cross-section⁵¹ are given by the equations below:

$$\alpha = -4\pi\epsilon_{\text{effs}}a^3B_{11} \quad (6)$$

$$C_{\text{abs}} = k\text{Im}[\alpha] \quad (7)$$

where k is the propagation constant and C_{abs} is the absorption cross-section.

The size of the particle falls under a quasi-static regime to approximate the larger contribution from absorption than scattering. The LSPR peak position obtained from computation is well predicted by the proposed model (Fig. S7, ESI†). This predicts a strong effect of image charge or Coulomb interaction on the observed trend in SERS enhancement.

Conclusions

The influence of the substrate on the plasmonic resonance of the nanoparticle does not entirely depend on the optical properties of the base substrate. The optical properties of the spacer play a significant role in the energy transfer from metal nanoparticles, especially for spacers thinner than 10 nm. Calculations were performed by introducing a substrate with effective permittivity including both the base substrate and spacer permittivity. An analytical model was also formulated to calculate the effect of Coulomb interaction in these substrates that can supplant other cumbersome mathematical approaches.^{40,41} This model predicts gains close to the experimental gains and the computationally intensive COMSOL numerical model. Based on the experimental observations, silver nanoparticles on 5 nm of Si_3N_4 on a Si base substrate showed optimum performance with a SERS enhancement of 10^5 for the detection of PNP and R6G. Thus we demonstrate a very simple, scalable wafer level processing technique to create sensitive SERS substrates without resorting to the nanolithography process.

Acknowledgements

This research was supported by the Department of Electronics and Information Technology (Deity), Govt. of India under CEN (Centre of Excellence in Nanoelectronics). Part of the research has been funded by Defence Research and Development Organisation (DRDO), Ministry of Defence. Siva Umamathy acknowledges the funding from the Department of Science and Technology (DST), Govt. of India.

References

- 1 A. J. Haes and R. P. Van Duyne, *Anal. Bioanal. Chem.*, 2004, **379**, 920–930.
- 2 C. Noguez, *J. Phys. Chem. C*, 2007, **111**, 3806–3819.
- 3 U. Kreibig and M. Vollmer, *Optical properties of metal clusters*, Springer Science & Business Media, 2013.
- 4 M. M. Miller and A. A. Lazarides, *J. Phys. Chem. B*, 2005, **109**, 21556–21565.
- 5 E. Le Ru and P. Etchegoin, *Chem. Phys. Lett.*, 2006, **423**, 63–66.
- 6 E. Le Ru, M. Meyer, E. Blackie and P. Etchegoin, *J. Raman Spectrosc.*, 2008, **39**, 1127–1134.
- 7 E. Le Ru, E. Blackie, M. Meyer and P. G. Etchegoin, *J. Phys. Chem. C*, 2007, **111**, 13794–13803.
- 8 P. Nordlander and E. Prodan, *Nano Lett.*, 2004, **4**, 2209–2213.
- 9 Y. Wu and P. Nordlander, *J. Phys. Chem. C*, 2009, **114**, 7302–7307.
- 10 S. Mubeen, S. Zhang, N. Kim, S. Lee, S. Krämer, H. Xu and M. Moskovits, *Nano Lett.*, 2012, **12**, 2088–2094.
- 11 C. Ciraci, R. Hill, J. Mock, Y. Urzhumov, A. Fernández-Domínguez, S. Maier, J. Pendry, A. Chilkoti and D. Smith, *Science*, 2012, **337**, 1072–1074.
- 12 T. Hutter, S. R. Elliott and S. Mahajan, *Nanotechnology*, 2013, **24**, 035201.

- 13 O. Glembocki, R. Rendell, D. Alexson, S. Prokes, A. Fu and M. Mastro, *Phys. Rev. B: Condens. Matter Mater. Phys.*, 2009, **80**, 085416.
- 14 M. W. Knight, Y. Wu, J. B. Lassiter, P. Nordlander and N. J. Halas, *Nano Lett.*, 2009, **9**, 2188–2192.
- 15 G. Xu, Y. Chen, M. Tazawa and P. Jin, *Appl. Phys. Lett.*, 2006, **88**, 043114.
- 16 S. Z. Malynych, N. L. Dmitruk and I. E. Moroz, *Eur. Phys. J.: Appl. Phys.*, 2013, **64**, 20402.
- 17 L. C. Shoute, A. J. Bergren, A. M. Mahmoud, K. D. Harris and R. L. McCreery, *Appl. Spectrosc.*, 2009, **63**, 133–140.
- 18 X. Rui, W. Xiao-Dong, L. Wen, X. Xiao-Na, L. Yue-Qiang, J. An, Y. Fu-Hua and L. Jin-Min, *Chin. Phys. B*, 2012, **21**, 025202.
- 19 A. O. Altun, S. K. Youn, N. Yazdani, T. Bond and H. G. Park, *Adv. Mater.*, 2013, **25**, 4431–4436.
- 20 G. Gupta, D. Tanaka, Y. Ito, D. Shibata, M. Shimojo, K. Furuya, K. Mitsui and K. Kajikawa, *Nanotechnology*, 2008, **20**, 025703.
- 21 D.-Y. Wu, B. Ren, Y.-X. Jiang, X. Xu and Z.-Q. Tian, *J. Phys. Chem. A*, 2002, **106**, 9042–9052.
- 22 M. Wind, J. Vlieger and D. Bedeaux, *Phys. A*, 1987, **141**, 33–57.
- 23 M. Wind, P. Bobbert, J. Vlieger and D. Bedeaux, *Phys. A*, 1987, **143**, 164–182.
- 24 M. Venkatapathi and A. K. Tiwari, *J. Appl. Phys.*, 2012, **112**, 013529.
- 25 O. S. Heavens, *Optical properties of thin solid films*, Courier Corporation, 1991.
- 26 D.-Y. Wu, X.-M. Liu, S. Duan, X. Xu, B. Ren, S.-H. Lin and Z.-Q. Tian, *J. Phys. Chem. C*, 2008, **112**, 4195–4204.
- 27 T. Tanaka, A. Nakajima, A. Watanabe, T. Ohno and Y. Ozaki, *Vib. Spectrosc.*, 2004, **34**, 157–167.
- 28 E. Ayars, H. Hallen and C. Jahncke, *Phys. Rev. Lett.*, 2000, **85**, 4180.
- 29 C. M. Aikens, L. R. Madison and G. C. Schatz, *Nat. Photonics*, 2013, **7**, 508–510.
- 30 M. Moskovits and J. Suh, *J. Phys. Chem.*, 1984, **88**, 5526–5530.
- 31 E. Le Ru, S. Meyer, C. Artur, P. Etchegoin, J. Grand, P. Lang and F. Maurel, *Chem. Commun.*, 2011, **47**, 3903–3905.
- 32 M. Muniz-Miranda, *Appl. Catal., B*, 2014, **146**, 147–150.
- 33 D. A. Perry, H. J. Son, J. S. Cordova, L. G. Smith and A. S. Biris, *J. Colloid Interface Sci.*, 2010, **342**, 311–319.
- 34 T. Tanaka, A. Nakajima, A. Watanabe, T. Ohno and Y. Ozaki, *J. Mol. Struct.*, 2003, **661**, 437–449.
- 35 P. Hildebrandt and M. Stockburger, *J. Phys. Chem.*, 1984, **88**, 5935–5944.
- 36 L. Jensen and G. C. Schatz, *J. Phys. Chem. A*, 2006, **110**, 5973–5977.
- 37 W. Yue, Z. Wang, Y. Yang, L. Chen, A. Syed, K. Wong and X. Wang, *J. Micromech. Microeng.*, 2012, **22**, 125007.
- 38 Z. Xu, H.-Y. Wu, S. U. Ali, J. Jiang, B. T. Cunningham and G. L. Liu, *J. Nanophotonics*, 2011, **5**, 053526.
- 39 J. Parker Jr, D. Feldman and M. Ashkin, *Phys. Rev.*, 1967, **155**, 712.
- 40 R. Ruppin, *Phys. Rev. B: Condens. Matter Mater. Phys.*, 1992, **45**, 11209.
- 41 Y. Eremin and N. Orlov, *Appl. Opt.*, 1996, **35**, 6599–6604.
- 42 P. Albella, B. Garcia-Cueto, F. González, F. Moreno, P. C. Wu, T.-H. Kim, A. Brown, Y. Yang, H. O. Everitt and G. Videen, *Nano Lett.*, 2011, **11**, 3531–3537.
- 43 R. Ruppin, *Surf. Sci.*, 1983, **127**, 108–118.
- 44 J. Lermé, C. Bonnet, M. Broyer, E. Cottancin, D. Manchon and M. Pellarin, *J. Phys. Chem. C*, 2013, **117**, 6383–6398.
- 45 V. V. Gozhenko, L. G. Grechko and K. W. Whites, *Phys. Rev. B: Condens. Matter Mater. Phys.*, 2003, **68**, 125422.
- 46 P. A. Letnes, I. Simonsen and D. Mills, *Phys. Rev. B: Condens. Matter Mater. Phys.*, 2011, **83**, 075426.
- 47 K. C. Vernon, A. M. Funston, C. Novo, D. E. Gómez, P. Mulvaney and T. J. Davis, *Nano Lett.*, 2010, **10**, 2080–2086.
- 48 J. M. Garnett, *Philos. Trans. R. Soc., A*, 1906, 237–288.
- 49 G. Piredda, D. D. Smith, B. Wendling and R. W. Boyd, *J. Opt. Soc. Am. B*, 2008, **25**, 945–950.
- 50 S. A. Maier, *Plasmonics: fundamentals and applications*, Springer Science & Business Media, 2007.
- 51 C. F. Bohren and D. R. Huffman, *Absorption and scattering of light by small particles*, John Wiley & Sons, 2008.